Alboresi Alessandro (Orcid ID: 0000-0003-4818-7778)
Morosinotto Tomas (Orcid ID: 0000-0002-0803-7591)

Front Matter

Title

Functional analysis of PsbS transmembrane domains through base editing in *Physcomitrium patens*.

Authors

Claudia Beraldo[1]†, Anouchka Guyon-Debast[2]†, Alessandro Alboresi[1], Fabien Nogué[2], Tomas Morosinotto [1]

Affiliations

1. Dipartimento di Biologia, Università di Padova, Padova, Italy.

2. Université Paris-Saclay, INRAE, AgroParisTech, Institut Jean-Pierre Bourgin (IJPB), 78000, Versailles, France.

† These authors contributed equally to this work

* Corresponding author, tomas.morosinotto@unipd.it

Abstract

Plants exposed to light fluctuations are protected from photodamage by non-photochemical quenching (NPQ), a reversible mechanism that enables dissipation of excess absorbed energy as heat, which is essential for plant fitness and crop productivity. In plants NPQ requires the presence of the membrane protein PsbS that, upon activation, interacts with antenna proteins, inducing their dissipative conformation. Here, we exploited base editing in the moss *Physcomitrium patens* to introduce *in vivo* specific amino acid changes and assess their impact on PsbS activity, targeting transmembrane regions to investigate their role in essential protein–protein interactions. This approach enabled the recognition of residues essential for protein stability and the identification of a hydrophobic cluster of amino acids impacting PsbS activity. This work provides new information on the PsbS molecular mechanism while also demonstrating the potential of base editing approaches for *in planta* gene function analysis.

RUNNING HEAD

PSBS KEY RESIDUES FOR PHOTOSYNTHESIS REGULATION

This article has been accepted for publication and undergone full peer review but has not been through the copyediting, typesetting, pagination and proofreading process which may lead to differences between this version and the Version of Record. Please cite this article as doi: 10.1111/tpj.16099

\MAIN TEXT

Introduction

Sunlight provides energy supporting the life of photosynthetic organisms through the activity of protein supercomplexes Photosystem (PS) I and II. In nature absorbed light often exceeds the metabolism capacity to use excitation energy, driving to the production of reactive oxygen species and the consequent photoinhibition (Li *et al.*, 2009). A feedback mechanism known as non-photochemical quenching (NPQ) drives the safe dissipation of excess excitation energy as heat, thus preventing photo-oxidative damage. Mutants unable to activate NPQ showed reduced fitness in outdoor conditions, suggesting that this regulatory mechanisms is particularly important for plant response to the highly dynamic conditions of natural environments (Kulheim *et al.*, 2002). While important under excess illumination, heat dissipation of excitation energy represents an energy loss and, if activated constitutively, it was shown to reduce photosynthetic efficiency and to negatively affect plant growth in limiting light conditions (Dall'Osto *et al.*, 2005). NPQ modulation thus must be optimal depending on the growing conditions with the balance between photoprotection and efficiency being essential for optimal productivity (Alboresi *et al.*, 2019). It was indeed shown that optimization of NPQ kinetics can drive an increased biomass productivity in tobacco and soybean plants in field conditions (Kromdijk *et al.*, 2016; De Souza *et al.*, 2022), confirming the major impact of this mechanisms on plant metabolisms while also demonstrating that the photosynthetic productivity can be improved in crops through genetics (Ort *et al.*, 2015).

NPQ activation is triggered by the decrease of pH in the lumen of thylakoids, a condition typically occurring when light absorption is higher than cell metabolic capacity to use absorbed energy for photochemistry. In plants, NPQ activation requires a thylakoid membrane protein, PsbS (Li *et al.*, 2000; Li *et al.*, 2002), that is protonated in two key glutamate residues when lumen pH decreases (Li *et al.*, 2004). PsbS is a member of the Light Harvesting Complex (LHC) superfamily, but in contrast to most of these proteins, it does not bind several chlorophylls and carotenoids and thus it is not directly involved in the absorption of incident light (Fan *et al.*, 2015). PsbS activity, instead, relies on the interaction with other, pigment-binding, LHCs (Betterle *et al.*, 2009; Gerotto *et al.*, 2015; Nicol *et al.*, 2019). In fact PsbS, upon pH induced activation, causes a conformational change in antenna complexes, inducing a state capable of efficiently dissipating excitation energy as heat (Goral *et al.*, 2012; Ruban and Wilson, 2021). Consistently with this hypothesis, NPQ capacity is also largely affected by the absence of LHC (Lokstein *et al.*, 1993; Nicol *et al.*, 2019). PsbS does not appear to bind to a specific binding site within the PSII-LHC supercomplex (Caffarri *et al.*,

2009; Kereïche *et al.*, 2010; McKenzie *et al.*, 2020; Gerotto *et al.*, 2015) suggesting it can interact with multiple LHC proteins.

Available knowledge on NPQ mechanism, thus, points to *in vivo* interactions between PsbS and LHCs as essential for its activation. Such interactions requires intact functional thylakoid membranes and they depend from generation of a proton gradient and are thus are only partially reproducible *in vitro* (Wilk *et al.*, 2013; Nicol and Croce, 2021), limiting available experimental approaches and impairing full functional analyses of the PsbS protein structure and identification of residues essential for activity. This makes *in vivo* studies essential to obtain deeper knowledge on PsbS structure and function, also to open any possibility of identifying modified versions of the protein with altered activity to modulate plant fitness and optimization of biomass production.

This question was addressed in this study using the moss Physcomitrella (*Physcomitrium patens*) as a model organism. In this organism NPQ depends on PsbS (Alboresi *et al.*, 2010), mutant generation is rapid and most tissues are haploid, making the phenotype assessment faster than in vascular plants by avoiding the need of waiting for the progeny. Furthermore, methods for precise base editing have been set up and validated showing high editing efficiency (Guyon-Debast *et al.*, 2021), providing a powerful tool and making *P. patens* a suitable organism for the *in vivo* study of PsbS variants. In this work, we employed advanced genome editing approaches based on CRISPR–Cas technology, namely cytosine base editor (CBE) and adenine base editor (ABE), to introduce specific nucleotide changes and targeted genetic diversity in the *P. patens PsbS* gene. This approach enabled the generation of various PsbS variants at the amino acid level and to assess the impact of amino acids changes on PsbS *in vivo* activity. Their functional analysis drove the identification of key residues for protein structure as well as a cluster of hydrophobic amino acids influential on protein activity, also demonstrating the power of the approach for precise genetic engineering and gene function analysis.

Results

In contrast to vascular plants, NPQ activation in the moss *P. patens* depends on two different proteins with additive contributions, PsbS and LHCSR (Gerotto *et al.*, 2012; Alboresi *et al.*, 2010). For this reason, to straightforwardly evaluate the impact on NPQ of changes in the PsbS sequence, *PsbS* mutagenesis was performed in a *lhcsr1* knock out background. These plants miss the most expressed LHCSR isoform while they still retain a second LHCSR isoform with a lower expression, thus enabling to clearly observe the PsbS impact on NPQ activation (Figure S1) (Alboresi *et al.*,

2010). 7 sgRNAs were designed to target the 4 transmembrane helices of PsbS with the base editing mutagenesis (Figure 1A, Table S1), following the hypothesis that these should play an important role as the sites of interaction with other integral membrane proteins, such as LHCs, which are essential for NPQ activity (Lokstein *et al.*, 1993; Nicol *et al.*, 2019). *lhcsr1* KO plants were transiently transformed using a vector expressing one Cas9 nickase fused either to a cytosine or an adenine deaminase base-editor (CBE and ABE, respectively) together with one or multiple sgRNAs (Figure S2).

After transient selection on antibiotic containing medium and regeneration, over 300 plants transfected by the CBE and ABE systems using multiplex or simplex strategies were genotyped by PCR (Figure S3). The *PsbS* gene of 265 plants (78% of regenerated plants) showed the expected WT- like size (e.g. variant #2, Figure S3) with no obvious chimerism or large deletions, which were otherwise observed in the other cases (e.g. variant #28 showed chimerism and variant #3 showed a large deletion, Figure S3). As observed previously (Guyon-Debast *et al.*, 2021), deletions were mostly detected in lines generated with multiplex strategy, driven by the simultaneous targeting of multiple sgRNAs (Figure S3). PCR-amplified fragments with expected apparent molecular weight were all sequenced. Out of those 265 independent plants, 163 showed an unaltered *PsbS* WT sequence (62%), whereas 102 showed some sequence modification (38%). In total, 65 plants (25% of plants with sequenced gene) showed different combinations of edited bases (Table S2), whereas some short indels and chimerism were detected in 8% and 5% of plants, respectively (Figure 1B). Overall, the BE system enabled to isolate 25 different variants of the PsbS protein with 1- to 5-amino acid changes, confirming that the approach was highly effective in generating a large set of genetic variants (Figure 1C-D and Table S3).

The genetic variants showed modification of 19 amino acids distributed over target protein regions (Figure 1D and Table S3). All modified amino acids but two (L123 and T128) are fully conserved in the *PsbS* sequence of *P. patens* and those of other angiosperms, making the phenotypes observed translatable to other species (Figure S4, Table S4). A more detailed analysis shows that multiplex and simplex strategies gave different results since the former yielded greater variability while the latter drove to isolation of plants with only 1-2 edited bases but with a much larger fraction of lines with WT sequences (Table S2).

All generated plants were phenotypically screened using a chlorophyll *a* fluorescence imaging apparatus to assess NPQ (Figure 2). The data showed that different lines had variable NPQ activity, demonstrating the power of the approach in generating functional variability (Figure 2). Indeed, if

some lines showed PsbS-WT like phenotype (e.g. line#51, Figure 2), several others had NPQ activity comparable to *psbs* KO plants (e.g. line#69, Figure 2) or an intermediate phenotype (line #53). All plants were subsequently subcloned, starting from a small portion of tissue to ensure genetic homogeneity and avoid propagating possible chimeras. For all plants carrying one or more edited bases, the *PsbS* locus was sequenced again after a second round of subclone isolation to confirm their genotype. In total, 25 PsbS variants (corresponding to 34 edited lines, Table 1 and Table S2), 1 line with silent mutation (line#102), 7 lines with deletions (3 in-frame and 4 non-in-frame) were used for full functional analysis. PsbS accumulation and activity were measured for all 25 PsbS variants; qE activity was also calculated as reported in Table 1.

6 additional lines obtained from the genome editing strategy but showing *PsbS* WT sequence were also randomly selected and included (Table S2). They all showed NPQ equivalent to the parental line (Figure S5A), demonstrating an optimal consistency between genotype and phenotype and that the approach did not drive to significant generation of undesired variability in the phenotype analyzed. On the other hand, all plants with deletions in the *PsbS* gene showed abolished protein accumulation resulting from failed import or stability and, consequently, impaired NPQ, which is similar to the *lhcsr1 psbs* KO line (Figure S5B-C), with the residual NPQ activity attributable to LHCSR2 isoform. Defective PsbS accumulation was even observed for the smallest deletions, like in ΔL147-L155, that is missing only 9 amino acids in the second transmembrane helix (line #201, Table S2, and Figure S5B-C).

In a few cases, base editing introduced a premature stop codon (Table S2, lines in pink); the latest stop codons found in the coding sequence were Q236* and L237*, which caused the loss of the 4th transmembrane helix (Figure S6). These plants showed no detectable protein accumulation or NPQ activity, demonstrating that this transmembrane helix and the C-terminal region are essential for PsbS protein stability and activity.

A complete lack of accumulation of PsbS protein was also observed in all PsbS variants carrying 3, 4 or 5 mutations (9 lines, table S2) and they all showed complete loss of NPQ activity (Figure S7). This finding suggests that multiple mutations increase the probability of driving protein destabilization with a consequent loss of activity.

PsbS variants carrying only one or two modified aminoacids, on the other hand, showed different NPQ phenotypes and protein accumulation. In some cases (e.g., G225sil, I227V G125K, G125A, Figure 3), no significant alteration in protein activity or accumulation was noted, and the base-edited plant NPQ phenotype was indistinguishable from the WT. These results could be due to the

conservative nature of sequence modification (G225sil, I227V, G125A) or to a small influence of the mutated residues on protein activity such as G125K or G125E.

In other cases, mutations caused strong protein destabilization with a major reduction in PsbS accumulation and consequent loss of NPQ activity. In L123P, the mutation into proline likely drives to destabilization of the alpha-helix structure, affecting the overall protein folding (Figure 4A-B). A similar phenotype was also observed in G125R-G127S plants that showed lower PsbS accumulation and no measurable NPQ activity (Figure 4A-B). Given that other single G125 mutants have no phenotypic alterations, this observation is likely attributable to G127, where the substitution with S can generate an electrostatic repulsion with E121 from TM1, destabilizing the protein. Another group of mutants, carrying different mutations in position R108 (R108P-G125K line#126, G107N-R108H line#197, G107D-R108H line#198, G107A-R108L line#199, Table S2) showed no PsbS accumulation and, consequently, NPQ activity. This observation strongly suggests to a major role of R108 on protein stability and activity since any substitution showed a strong impact (Figure 4C-D).

The analysis of some single and double mutants showed different levels of PsbS destabilization with a lower PsbS accumulation correlated with decrease in NPQ activity (Figure 5). As example, the substitution of tyrosine with isoleucine in position 154 (Figure 5A, Table S2 line#206,#53) had minor impact on PsbS activity and accumulation, both in the single T154I mutant and in the G107A-T154I double mutant. Instead, a larger destabilization was observed in Q236R (Figure 5B, Table S2 line#196, line#205), R165H (Figure 5C, Table S2 line#194) single mutant and even larger in D164N-R165H double mutant (Figure 5C, Table S2 line#200). In all cases, the reduction in protein abundance corresponded to a decrease in NPQ activity.

Interestingly, another set of mutants showed a significant alteration in NPQ activity (Figure 6A-B), whereas PsbS accumulation was maintained (Figure 6C, Figure S9), suggesting an alteration in protein activity. The F153L mutation in particular showed lower NPQ, a phenotype confirmed when measuring with both, saturating and non-saturating actinic light (Figure 6A-B). F153L effect was also confirmed by other mutants carrying the same mutation in combination with changes in G125 (G125K/Q), which was already shown to have no impact on activity (Figure 3).

Discussion

Base editing approaches are effective in generating genetic variability for functional analyses.

PsbS protein activity requires a low pH in the lumen, as well as interactions with photosystem complexes (Betterle *et al.*, 2009) and thus it can only be properly measured *in vivo* and base editing (BE) represents a valuable tool to obtain new information on its molecular mechanisms and functional role of key residues. The BE approach applied here in *P. patens* was successful in generating a large set of plants with variable modifications in the PsbS sequence, carrying 1-5 amino acid variants or deletion of different size. Despite the fact that plants were only transiently transfected with constructs driving gene editing, the BE system was active in more than one-third of plants, and enabled the generation of 25 different variants of the PsbS protein with 1- to 5-amino acid changes, confirming that the approach was effective in generating a large set of genetic variants (Figure 1C and Table S2).

Both multiplex (using multiple gRNA) and simplex (with a single gRNA) strategies were effective in generating mutations in the expected regions, even though the approaches yielded different results. Lines obtained using multiplex transformation exhibited greater variability but, on the other hand, were also enriched in lines with deletions and a large number of mutations (> 3) that in both cases caused complete destabilization of protein structure and thus finally provided less biological information. The simplex approach, instead, only yielded plants with 1-2 edited bases but, at the same time, also had a much larger fraction of lines with WT sequences (Figure 1 and Table S2).

In analyzing those efficiencies, however, it should be underlined that the binding efficiency of each sgRNA is variable and plays a major influence on the results obtained, as shown by the different frequency of mutations found in the targeted regions. Here the simplex strategy was only performed for those sgRNAs shown to be less effective in earlier multiplex experiments to enrich variants in those protein regions and this likely cause an enriched increase in frequency of lines with WT sequence.

It is also interesting to observe that all lines with no alterations in PsbS coding sequence (Figure S5A) or that carried silent mutations (Figure 3A-3C), variant *psbs*G225sil), all have phenotype indistinguishable from parental line. Since NPQ levels are very sensitive to PsbS accumulation levels (Gerotto *et al.*, 2011). This observation suggests the mutagenesis was very specific in targeting coding sequences and did not affect the expression levels of target proteins.

Concerning the possible generalization of the approach to study other genes / biological processes, it should be considered that PsbS activity can be measured simultaneously on multiple plants using fluorescence imaging systems (Figure 2), which strongly facilitate the screening of a large number

of lines and the rapid selection of the most interesting phenotypes. On the other hand, in the present work we decided not to discard any lines based on the fluorescence screening and there were all subjected to genotype assessment. In consequence, the same strategy could potentially be applied for functional analysis of other genes even if the screening of the activity of their encoded proteins is not as easily measurable.

Considering the CRISPR flexibility, the approach described could be applied to many different model organisms. The choice of working with the moss *P. patens*, however, provided advantages in the speed of generation, selection, and characterization of lines since transfected plants can be assessed genotypically and phenotypically approx. 3 months after transformation without the need of any crossing. In the case of *P. patens* proteins showing high sequence similarity with vascular plants, as is the case of PsbS here, the results are expected to be largely transferable between species and thus the choice of *P. patens* as a model provides a significant advantage to obtain fast results and increase the size of the population of genetic variants that can be analyzed.

Identification of ionic bridges essential for PsbS stability

Among the lines carrying a limited number of aminoacid modifications, some of them showed a strong impact on protein accumulation. In all cases, a strong impairment of PsbS accumulation drove to an impairment of NPQ activity that however does not imply any specific involvement of the residues in activation mechanism. As example, Q236 is located in H2 and it forms polar interactions with K231 and S222 in TM3 (Figure S8A) that are likely altered by Q236R, causing protein destabilization and highlighting the relevance of this polar interaction for protein stability.

Other examples are D164 and R165, located at the stromal part of TM2. The R165 carbon backbone interacts with F98 and K100, but these interactions are expected to be maintained in the mutants as well. The R165H mutation should instead impair polar interactions with G97 (Figure S8B). D164 stabilizes polar interactions with K100 and R213 (Figure S8B) in TM1 and 3, respectively, likely lost in mutant D164N. Both D164 and R165 are conserved in vascular plants (Table S4), and these interactions are thus expected to be very relevant for the stabilization of protein structure, as confirmed by the strong impact of a mild modification such as D164N (Figure S8B). Overall, these results point to electrostatic interactions in the stromal part of the protein as seminal for PsbS structural organization.

Another example or residue with a strong impact is R108, that is part of a conserved transmembrane sequence typical of all LHC superfamily members. R is a hydrophilic residue and its presence in an hydrophobic part of the protein is possible because it is involved in a salt bridge with the glutamic acid of another transmembrane helix, essential to stabilize the structure and equilibrate the charge (Liu *et al.*, 2004; Remelli *et al.*, 1999). A corresponding PsbS mutant in *A. thaliana* was already tested, showing NPQ impairment consistent with results presented here (Schultes and Peterson, 2007). Structural investigation shows that R108 interacts with E208 on TM3 but also with A263 and N265 in TM4 (Figure 7). In other LHCs the transmembrane glutamic acid instead coordinates the Mg^{2+} of a chlorophyll (Figure 8), which is absent in PsbS. The extra partners for electrostatic interactions of the glutamate, likely essential since this is a membrane region where unbalanced electrostatic charges would cause a large energetic penalty, in PsbS are instead found in TM4. The two mutations Q236* and L237* reinforce the idea that TM4 is indeed essential for PsbS protein stability. It is interesting to observe that PsbS is the only member of the LHC multigenic family with a fourth transmembrane helix and thus this network of electrostatic interaction is specific to this protein and likely connected with its intrinsic properties and its specialized role in NPQ activation. These results suggest that, despite their common ancestral origin, structural organizations in PsbS and antenna proteins diverged, likely in correlation with different pigments binding properties and ultimately functions.

Identification of a hydrophobic cluster possibly involved in PsbS – antenna interactions.

F153L either alone or in combinations with other mutations showed a small reduction of NPQ activity without significantly affecting PsbS protein accumulation, suggesting a less effective PsbS protein. Given that both leucine and phenylalanine have hydrophobic properties, the reduction in the activity of the F153L mutant cannot be attributed to a protein destabilization but rather to the absence of the aromatic ring, which may be involved in hydrophobic interactions. F153 is located in the second transmembrane helix (Figure 8) and in the 3D structure is found close to F149 and F150 (TM2), V106 (TM1), F98 (TM1) and L162 (TM2). All these hydrophobic and aromatic residues (Figure 8) are well conserved in different organisms (Figure S4), suggesting a possible functional role beyond the hydrophobicity required for membrane embedding.

This cluster of hydrophobic amino acids is not involved in intermolecular interactions within the PsbS dimer but it protrudes from the protein, pointing toward the membrane (Figure 8). In the PsbS structure, F153 and other residues of this hydrophobic cluster interacts with n-nonyl-β-D-glucopyranoside (BNG), the detergent used for protein isolation before crystallization (Fan *et al.*,

2015), suggesting these residues are available for hydrophobic interactions within the thylakoids membrane. These findings suggest that *in vivo* these residues could interact with other hydrophobic components present in the membrane, such as lipids or antenna proteins, and that these interactions may indeed have an important functional role.

Even though F153L impact is small, this is consistent with a diffused interaction between PsbS and its interactors involving multiple residues, each providing a contribution. This is also consistent with PsbS not having a specific binding site with antennas but showing some promiscuity of interaction with different antennas (Gerotto *et al.*, 2015). Although further evidence is needed, all data presented here and in the literature, including the elusive nature of PsbS interactors, are consistent with the hydrophobic group of amino acids identified here being involved in the interaction between the PsbS and the antennas.

Materials and Methods

Molecular cloning. Guide RNA (sgRNA) sequences specific to the *PsbS* gene (Pp3c20_23430) were chosen using the web tool CRISPOR 4.97 (Concordet & Haeussler, 2018). Expression cassettes sgRNA#5, sgRNA#57, sgRNA#176, sgRNA#180, sgRNA#396, sgRNA#426 and sgRNA#507, including the promoter of the *P. patens* U6 snRNA (Collonnier *et al.*, 2017), the 5'-G-N(19)-3' guide sequences targeting the *PsbS* gene and the tracrRNA scaffold, were synthesized by Twist Bioscience (San Francisco, California, USA; Table S1). Expression cassettes were subcloned into the pDONR207-NeoR vector(Guyon-Debast *et al.*, 2021) by Gateway™ BP reaction (Invitrogen) as previously described to yield psgRNA#5, psgRNA#57, psgRNA#176, psgRNA#180, psgRNA#396, psgRNA#426 and psgRNA#507. For the CBE and ABE systems, we used the plasmids pnCas9-CBE1 (pAct-nCas9-CBE) and pnCas9-ABE1 (pAct-nCas9-ABE), as previously described (Guyon-Debast *et al.*, 2021).

Moss culture and transformation. Plants were grown on $PpNH_4$ medium ($PpNO_3$ medium supplemented with 2.7 mM NH_4-tartrate) in growth chambers set at 60% humidity with 16 hours of light (quantum irradiance of 40 µmol m^{-2} s^{-1}) at 24 °C and 8 hours of dark at 22 °C. Moss protoplast isolation from *lhcsr1* KO plants and transfection were performed as previously described (Charlot *et al.*, 2022). Protoplasts were transfected with a total of 21 µg of circular DNA divided as follows: 7 µg of each base editor (pnCas9-CBE1 and pnCas9-ABE1 plasmids) and a mix of 7 µg of sgRNA plasmids for multiplex or 10 µg of the base editor (pnCas9-CBE1 or pnCas9-ABE1 plasmid) and 10 µg of the sgRNA plasmid (psgRNA#5, psgRNA#176, psgRNA#180,

psgRNA#396 or psgRNA#426). After protoplast regeneration, plants were transferred to $PpNH_4$ supplemented with 50 mg/L G418 (Duchefa) to select clones that were transiently transfected (Figure S2). A total of 189 transfected plants were selected using the multiplex strategy. To produce some additional specific genetic combinations, 151 transfected plants were selected using the simplex strategy. *lhcsr1* KO plants were used here to avoid the interference of LHCSR- over PsbS-dependent activity, the selection in *lhcsr1 lhcsr2* KO plants was not feasible since they are already resistant to antibiotic G418 (Alboresi *et al.*, 2010).

PCR and sequence analysis of the edited plants. For PCR analysis of transiently transfected plants, genomic DNA was extracted from 50 mg of fresh tissue as previously described (Lopez-Obando *et al.*, 2016). Molecular analysis was based on PCR genotyping using primers surrounding the targeted locus, F1 and R1 primers. Sanger sequencing (Genoscreen, Lille, France) of the *PsbS* gene was performed on 265 plants showing no large deletion or obvious chimerism. The exon 1 sequence was also checked using the F2 and R2 primers for the 67 edited plants. The PCR primers used in this study are listed in Table S2.

In vivo Chl fluorescence kinetics. For screening purposes, the *in vivo* chlorophyll fluorescence signal was monitored at room temperature with an imaging instrument, FluorCam 800-C (Photon System Instruments). Approximately one-month-old plants were exposed after a dark adaptation to actinic light (850 µmol photons m^{-2} s^{-1}) for 4 minutes and then left to recover for an additional 4 minutes and 12 seconds in the dark.

After selection, the NPQ phenotype was assessed by the *in vivo* chlorophyll fluorescence signal at room temperature with a Dual-PAM-100 fluorometer (Walz, Germany) in protonemal tissues grown for 10 days in $PpNO_3$ medium under control growth conditions (40 µmol m^{-2} s^{-1}). Before measurements, plants were dark-acclimated for 40 minutes. For induction kinetics, actinic light was set to 850 (saturating actinic light) or 330 µmol photons $m^{-2} \cdot s^{-1}$. PSII parameters were calculated as follows: Fv/Fm as (Fm − Fo)/Fm and NPQ as (Fm − Fm′)/Fm′. Data are presented as the mean ± SD of at least 3 independent experiments.

Total protein extracts, SDS page, and Immunoblotting. For Western blot analysis, 6 independently transfected plants (#11, 115, 154, 162, 177, 190) showing the *psbs* WT sequence were used as a reference given that PsbS WT from transfected plants had the same PsbS accumulation as the parental line. In addition, 7 independently transfected plants with deletions in the *psbs* sequence (# 18, 56, 81, 142, 143, 201, 202) were used as a reference given that lines with deletions in PsbS exhibited no PsbS accumulation, which is similar to that noted for the *psbs* KO line generated from homologous recombination (Figure S5). Total extracts were obtained by grinding tissues in sample

buffer before SDS/PAGE. For immunoblotting analysis, after SDS/PAGE, proteins were transferred to nitrocellulose membranes (Pall Corporation) and detected with a specific homemade polyclonal PsbS antibody (Gerotto *et al.*, 2015). The Chl a/b and Chl/Car ratios were obtained by fitting the spectrum of 80% acetone pigment extracts with spectra of the individually purified pigments (Croce *et al.*, 2002).

References

Alboresi, A., Gerotto, C., Giacometti, G.M., Bassi, R. and Morosinotto, T. (2010) Physcomitrella patens mutants affected on heat dissipation clarify the evolution of photoprotection mechanisms upon land colonization. *Proc. Natl. Acad. Sci. U. S. A.*, **107**, 11128–33. Available at: http://www.pnas.org/cgi/doi/10.1073/pnas.1002873107 [Accessed February 19, 2020].

Alboresi, A., Storti, M. and Morosinotto, T. (2019) Balancing protection and efficiency in the regulation of photosynthetic electron transport across plant evolution. *New Phytol.*, **221**, 105–109. Available at: http://doi.wiley.com/10.1111/nph.15372 [Accessed July 2, 2020].

Betterle, N., Ballottari, M., Zorzan, S., Bianchi, S. de, Cazzaniga, S., Dall'Osto, L., Morosinotto, T. and Bassi, R. (2009) Light-induced dissociation of an antenna hetero-oligomer is needed for non-photochemical quenching induction. *J. Biol. Chem.*, **284**, 15255–15266. Available at: http://www.scopus.com/inward/record.url?eid=2-s2.0-67649304885&partnerID=tZOtx3y1 [Accessed November 5, 2014].

Caffarri, S., Kouril, R., Kereïche, S., Boekema, E.J. and Croce, R. (2009) Functional architecture of higher plant photosystem II supercomplexes. *EMBO J.*, **28**, 3052–63. Available at: http://www.scopus.com/inward/record.url?eid=2-s2.0-70350565366&partnerID=tZOtx3y1 [Accessed November 26, 2014].

Charlot, F., Goudounet, G., Nogué, F. and Perroud, P.-F. (2022) Physcomitrium patens Protoplasting and Protoplast Transfection. In pp. 3–19.

Collonnier, C., Epert, A., Mara, K., Maclot, F., Guyon-Debast, A., Charlot, F., White, C., Schaefer, D.G. and Nogué, F. (2017) CRISPR-Cas9-mediated efficient directed mutagenesis and RAD51-dependent and RAD51-independent gene targeting in the moss *Physcomitrella patens*. *Plant Biotechnol. J.*, **15**, 122–131. Available at:

http://www.ncbi.nlm.nih.gov/pubmed/27368642 [Accessed August 7, 2018].

Croce, R., Canino, G., Ros, F. and Bassi, R. (2002) Chromophore Organization in the Higher-Plant Photosystem II Antenna Protein CP26. *Biochemistry*, **41**, 7334–7343. Available at: http://www.scopus.com/inward/record.url?eid=2-s2.0-0037062584&partnerID=tZOtx3y1 [Accessed November 26, 2014].

Dall'Osto, L., Caffarri, S. and Bassi, R. (2005) A mechanism of nonphotochemical energy dissipation, independent from PsbS, revealed by a conformational change in the antenna protein CP26. *Plant Cell*, **17**, 1217–32. Available at: http://www.scopus.com/inward/record.url?eid=2-s2.0-23744439566&partnerID=tZOtx3y1 [Accessed December 5, 2014].

Fan, M., Li, M., Liu, Z., Cao, P., Pan, X., Zhang, H., Zhao, X., Zhang, J. and Chang, W. (2015) Crystal structures of the PsbS protein essential for photoprotection in plants. *Nat. Struct. Mol. Biol.*, **22**, 729–735.

Gerotto, C., Alboresi, A., Giacometti, G.M.G.M., Bassi, R. and Morosinotto, T. (2011) Role of PSBS and LHCSR in Physcomitrella patens acclimation to high light and low temperature *Plant, Celle Environ.*, **34**, 922–932. Available at: https://www.scopus.com/record/display.uri?eid=2-s2.0-79955730463&origin=inward&txGid=bdefdafa2943e1c75160c72993180c02 [Accessed November 24, 2014].

Gerotto, C., Alboresi, A., Giacometti, G.M.G.M., Bassi, R. and Morosinotto, T. (2012) Coexistence of plant and algal energy dissipation mechanisms in the moss Physcomitrella patens. *New Phytol.*, **196**, 763–73. Available at: http://www.scopus.com/inward/record.url?eid=2-s2.0-84867405489&partnerID=tZOtx3y1 [Accessed November 24, 2014].

Gerotto, C., Franchin, C., Arrigoni, G. and Morosinotto, T. (2015) In Vivo Identification of Photosystem II Light Harvesting Complexes Interacting with PHOTOSYSTEM II SUBUNIT S. *Plant Physiol.*, **168**, 1747–61. Available at: http://www.scopus.com/inward/record.url?eid=2-s2.0-84939196603&partnerID=tZOtx3y1 [Accessed January 7, 2016].

Goral, T.K., Johnson, M.P., Duffy, C.D.P., Brain, A.P.R., Ruban, A. V and Mullineaux, C.W. (2012) Light-harvesting antenna composition controls the macrostructure and dynamics of thylakoid membranes in Arabidopsis. *Plant J.*, **69**, 289–301. Available at:

http://www.ncbi.nlm.nih.gov/pubmed/21919982 [Accessed November 21, 2014].

Guyon-Debast, A., Alboresi, A., Terret, Z., et al. (2021) A blue-print for gene function analysis through Base Editing in the model plant Physcomitrium (Physcomitrella) patens. *New Phytol.* Available at: http://www.ncbi.nlm.nih.gov/pubmed/33421132 [Accessed January 21, 2021].

Kereïche, S., Kiss, A.Z., Kouril, R., Boekema, E.J. and Horton, P. (2010) The PsbS protein controls the macro-organisation of photosystem II complexes in the grana membranes of higher plant chloroplasts. *FEBS Lett.*, **584**, 759–64. Available at: http://www.scopus.com/inward/record.url?eid=2-s2.0-77649273780&partnerID=tZOtx3y1 [Accessed November 2, 2014].

Kromdijk, J., Głowacka, K., Leonelli, L., Gabilly, S.T., Iwai, M., Niyogi, K.K. and Long, S.P. (2016) Improving photosynthesis and crop productivity by accelerating recovery from photoprotection. *Science*, **354**, 857–861. Available at: http://www.ncbi.nlm.nih.gov/pubmed/27856901 [Accessed February 1, 2017].

Kulheim, C., Agren, J. and Jansson, S. (2002) Rapid Regulation of Light Harvesting and Plant Fitness in the Field. *Science (80-.).*, **297**, 91–94.

Li, X.-P., Muller-Moule, P., Gilmore, A.M. and Niyogi, K.K. (2002) PsbS-dependent enhancement of feedback de-excitation protects photosystem II from photoinhibition. *Proc. Natl. Acad. Sci. U. S. A.*, **99**, 15222–7. Available at: http://www.pnas.org/cgi/doi/10.1073/pnas.232447699 [Accessed January 28, 2021].

Li, X.P., Björkman, O., Shih, C., Grossman, A.R., Rosenquist, M., Jansson, S. and Niyogi, K.K. (2000) A pigment-binding protein essential for regulation of photosynthetic light harvesting. *Nature*, **403**, 391–5. Available at: http://www.ncbi.nlm.nih.gov/pubmed/10667783 [Accessed January 9, 2016].

Li, Y., Lucas, M.-G., Konovalova, T., et al. (2004) Mutation of the putative hydrogen-bond donor to P700 of photosystem I. *Biochemistry*, **43**, 12634–47. Available at: http://www.scopus.com/inward/record.url?eid=2-s2.0-1242314613&partnerID=tZOtx3y1 [Accessed November 26, 2014].

Li, Z., Wakao, S., Fischer, B.B. and Niyogi, K.K. (2009) Sensing and responding to excess light. *Annu. Rev. Plant Biol.*, **60**, 239–60. Available at: http://www.ncbi.nlm.nih.gov/pubmed/19575582 [Accessed September 7, 2014].

Liu, Z., Yan, H., Wang, K., Kuang, T., Zhang, J., Gui, L., An, X. and Chang, W. (2004) Crystal structure of spinach major light-harvesting complex at 2.72 Å resolution. *Nature*, **428**, 287–292. Available at: http://www.ncbi.nlm.nih.gov/pubmed/15029188 [Accessed October 1, 2015].

Lokstein, H., Härtel, H., Hoffmann, P. and Renger, G. (1993) Comparison of chlorophyll fluorescence quenching in leaves of wild-type with a chlorophyll-b-less mutant of barley (Hordeum vulgare L.). *J. Photochem. Photobiol. B Biol.*, **19**, 217–225. Available at: https://linkinghub.elsevier.com/retrieve/pii/1011134493870874 [Accessed January 28, 2021].

Lopez-Obando, M., Hoffmann, B., Géry, C., Guyon-Debast, A., Téoulé, E., Rameau, C., Bonhomme, S. and Nogué, F. (2016) Simple and Efficient Targeting of Multiple Genes Through CRISPR-Cas9 in Physcomitrella patens. *G3 (Bethesda).*, **6**, 3647–3653.

McKenzie, S.D., Ibrahim, I.M., Aryal, U.K. and Puthiyaveetil, S. (2020) Stoichiometry of protein complexes in plant photosynthetic membranes. *Biochim. Biophys. acta. Bioenerg.*, **1861**, 148141. Available at: http://www.ncbi.nlm.nih.gov/pubmed/31825808 [Accessed January 28, 2021].

Nicol, L. and Croce, R. (2021) The PsbS protein and low pH are necessary and sufficient to induce quenching in the light-harvesting complex of plants LHCII. *Sci. Rep.*, **11**, 7415. Available at: http://www.nature.com/articles/s41598-021-86975-9 [Accessed April 20, 2021].

Nicol, L., Nawrocki, W.J. and Croce, R. (2019) Disentangling the sites of non-photochemical quenching in vascular plants. *Nat. Plants*, **5**, 1177–1183. Available at: https://pubmed.ncbi.nlm.nih.gov/31659240/ [Accessed June 23, 2020].

Ort, D.R., Merchant, S.S., Alric, J., et al. (2015) Redesigning photosynthesis to sustainably meet global food and bioenergy demand. *Proc. Natl. Acad. Sci. U. S. A.*, **112**, 8529–36. Available at: http://www.pnas.org/lookup/doi/10.1073/pnas.1424031112 [Accessed October 29, 2018].

Remelli R, Varotto C, Sandonà D, Croce R, Bassi R. (1999) Chlorophyll binding to monomeric light-harvesting complex. A mutation analysis of chromophore-binding residues. *J Biol Chem.*, **274**, 33510-21. Available at: https://pubmed.ncbi.nlm.nih.gov/10559236/ [Accessed October 3, 2022].

Ruban, A. V. and Wilson, S. (2021) The Mechanism of Non-Photochemical Quenching in Plants: Localization and Driving Forces. *Plant Cell Physiol.*, **62**, 1063–1072. Available at: https://pubmed.ncbi.nlm.nih.gov/33351147/ [Accessed October 3, 2022].

Schultes, N.P. and Peterson, R.B. (2007) Phylogeny-directed structural analysis of the Arabidopsis PsbS protein. *Biochem. Biophys. Res. Commun.*, **355**, 464–470. Available at: https://pubmed.ncbi.nlm.nih.gov/17306227/ [Accessed October 12, 2021].

Souza, A.P. De, Burgess, S.J., Doran, L., et al. (2022) Soybean photosynthesis and crop yield are improved by accelerating recovery from photoprotection. *Science*, **377**, 851–854.

Wilk, L., Grunwald, M., Liao, P.-N., Walla, P.J. and Kühlbrandt, W. (2013) Direct interaction of the major light-harvesting complex II and PsbS in nonphotochemical quenching. *Proc. Natl. Acad. Sci. U. S. A.*, **110**, 5452–6. Available at: http://www.pnas.org/cgi/doi/10.1073/pnas.1205561110 [Accessed January 28, 2021].

Acknowledgments

Funding:

French National Research Agency (ANR11-BTBR-0001-GENIUS, FN).

Saclay Plant Sciences-SPS (ANR-17-EUR-0007, FN).

Author contributions:

Conceptualization: FN, AA, TM

Methodology: AA, FN, AGD

Investigation: CB, AGD, AA

Visualization: CB, AA, TM

Supervision: AA, FN, TM

Writing—original draft: TM

Writing—review & editing: CB, AGD, AA, FN

Competing interests: Authors declare that they have no competing interests.

Data and materials availability: All data are available in the main text or the supplementary materials.

Figures and Tables

Table 1. Base-edited variants of *PsbS*, and their effects on PsbS protein accumulation and function *in vivo*. Reference lines, *lhcsr1* KO PSBS WT (HR) and *lhcsr1 psbs* KO, are highlighted in grey. PsbS protein level was measured by immunoblotting, and the non-photochemical quenching (NPQ) phenotype was estimated by chlorophyll fluorescence measurements (with an actinic illumination of 850 µmol photons m^{-2} s^{-1}). qE was calculated as the difference between NPQ value at last light point of actinic light treatment (minute 8) and the NPQ value after 1 minute of dark relaxation (minute 9). A minimum of three different independent plants were tested for each variant. Ø indicates undetectable PsbS accumulation. "ns" indicates no significant differences between PSBS WT (HR) and mutant lines; asterisks indicate significant differences between PSBS WT lines and mutant lines (One-Way ANOVA test, $p < 0,01$).

# mutations (# variants)	PsbS variants	TM	Protein accumulation (% compared to WT)	qE value
parental line	WT		100%	0.37±0.03
psbs KO H.R.	KO		Ø	0.19±0.01
1 mutation (9 variants)	F153L	2	~100%	$0.33±0.6^{ns}$
	R165H	2	<10%	0.2± 0.03*
	I227V	3	~100%	$0.37±0.05^{ns}$
	Q236R	3	50%±20%	0.20±0.03*
	L123P	1	<10%	0.17±0.01*
	G125K	1	~100%	$0.32±0.07^{ns}$
	G125E	1	~100%	$0.3±0.01^{ns}$
	G125A	1	~100%	$0.41±0.05^{ns}$
	T154I	2	70%±20%	$0.28±0.03^{ns}$
2 mutations (9 variants)	G125K-F153L	1, 2	~100%	$0.34±\ 0.04^{ns}$
	G107N-R108H	1	Ø	0.17± 0.01*
	G107D-R108H	1	Ø	0.21±0.014*
	G107A-R108L	1	Ø	0.16±0.04*
	D164N-R165H	2	<10%	0.22± 0.01*
	G125R-G127S	1	Ø	0.13± 0.05*
	G125Q-F153L	1, 2	~WT	0.26±0.02*
	G107A-T154I	1, 2	70%±20%	$0.34±0.04^{ns}$
	R108P-G125K	1	<10%	0.11±0.04*
3 mutations (4 variants)	G125K-L155V-G225R	1, 2, 3	Ø	0.20±0.02*
	G107D-R108H-Q236E	1, 3	Ø	0.14±0.02*
	G107D-R108H-G125K	1, 2	Ø	0.1±0.07*
	G125K-T154I-Q236E	1, 2, 3	<10%	0.17±0.02*
4 mutations (1 variant)	G107N-R108H-G125K-R165H	1, 2	Ø	0.25±0.02*
5 mutations	G107A-R108L-G125K-F153L-R165H	1, 2	Ø	0.14±0.02*

(2 variants)	G107A-R108H-G125K-A262G-A263V	1, 4	Ø	0.13±0.01*

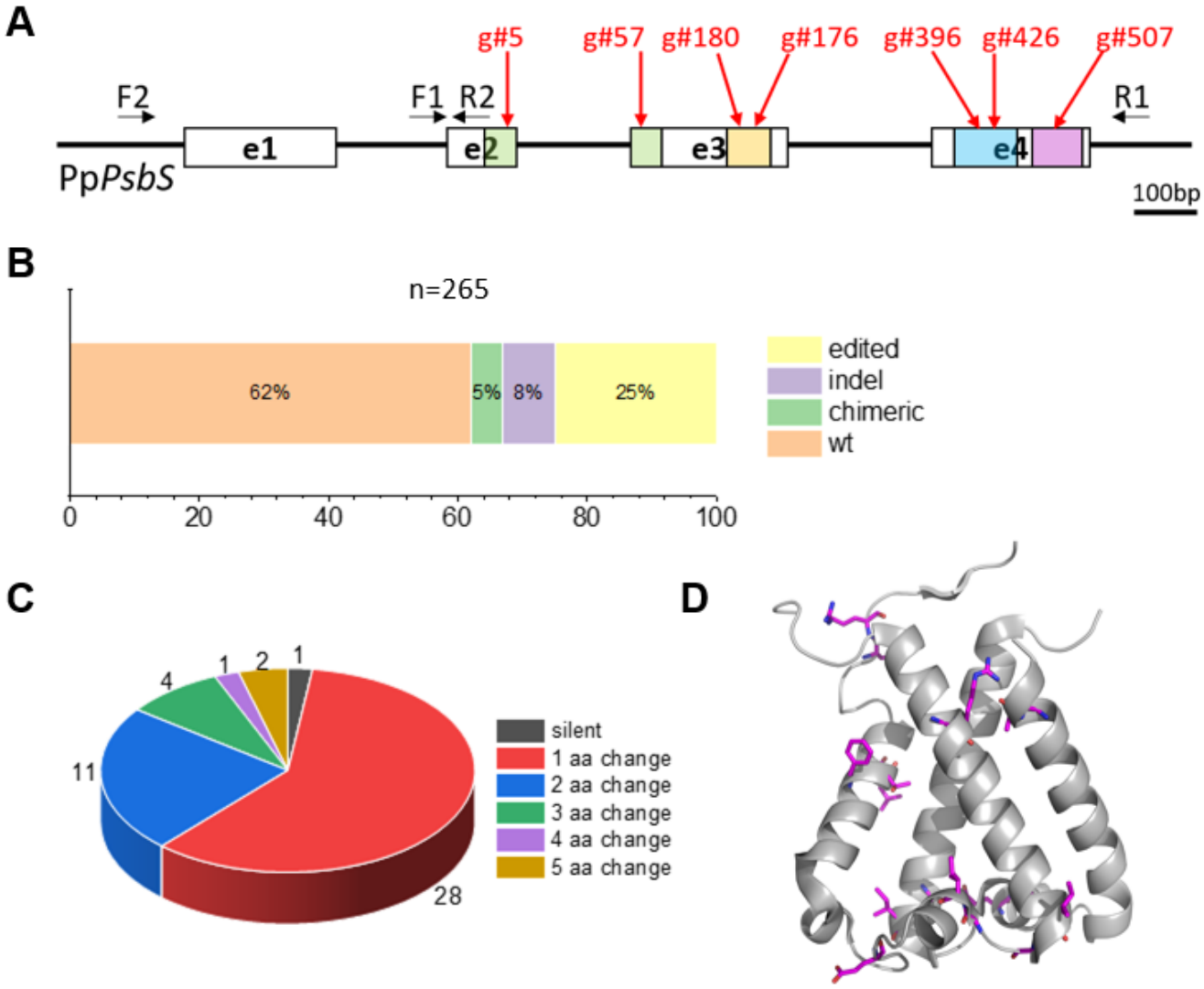

Figure 1. Base Editing to generate variants of PSBS protein. A) Scheme of the Pp*PsbS* gene and indication of regions targeted by sgRNAs. Boxes represent the exons (e1, e2, e3 and e4) and lines represent the introns. The coding sequence of the four transmembrane domains are indicated with colored boxes (green for TM1, yellow for TM2, blue for TM3 and purple for TM4). The seven sgRNAs positions are indicated by red arrows and the primers used for PCR and sequencing by black arrows. B) Results of Pp*PsbS* gene sequencing for the 265 transfected plants originated from both multiplex and simplex strategy. The 75 lines that showed chimerism or large deletions were not included. C) Number of amino acid changes identified in the edited plants. D) 3D structural model of PpPsbS with all edited aminoacids highlighted in magenta.

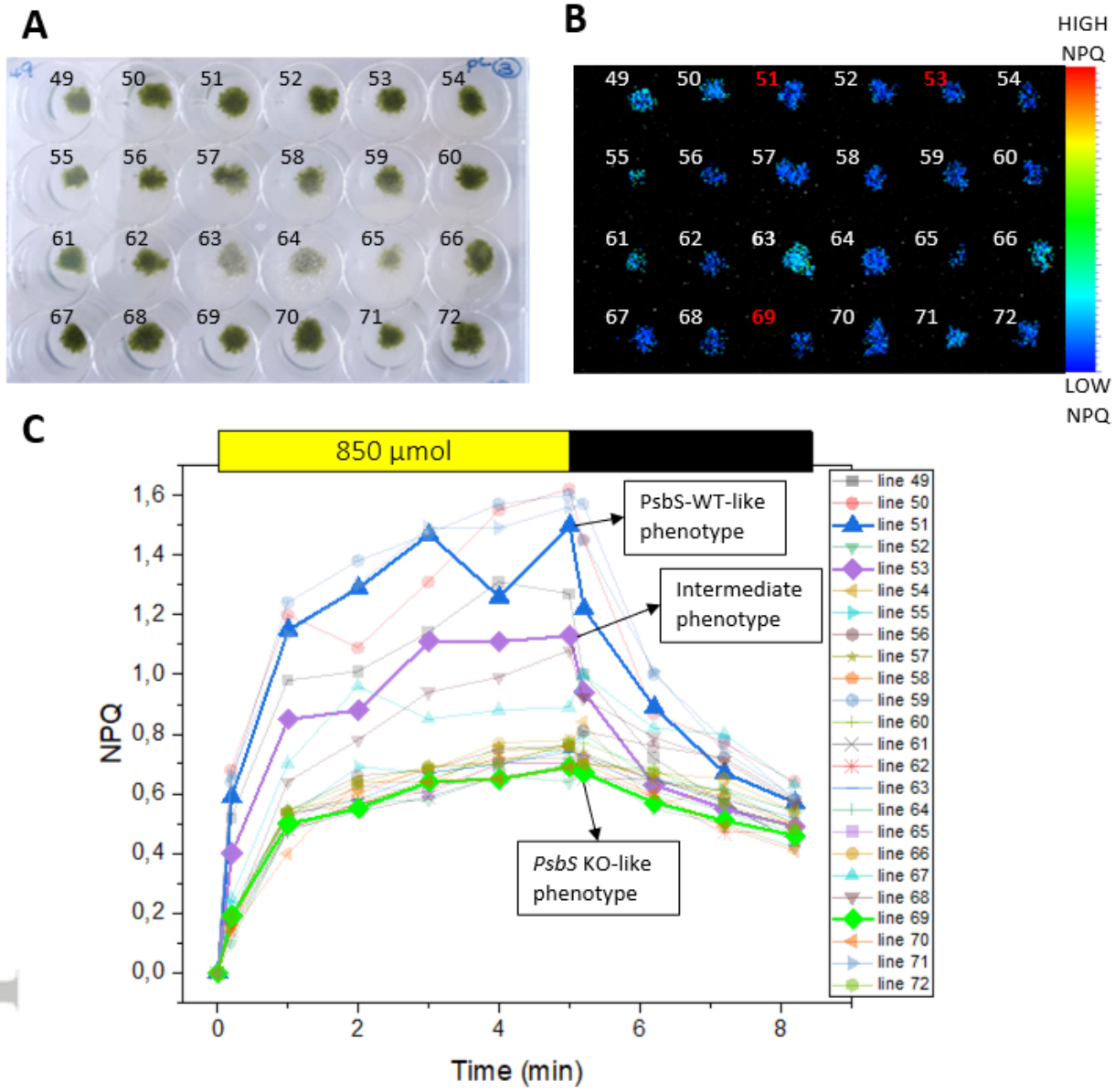

Figures 2. Example of screening of NPQ capacity in edited plants. Multiple independent lines (here the sub-group from #49 to #72) were obtained after *lhcsr1* KO protoplast transformation using multiplex and simplex strategies and then screened by chlorophyll fluorescence imaging. A) Representative 24-well plate used for the screening. B) NPQ levels of the same plants present in panel A, reported as false colors. Lines #51, #53, #69 are highlighted in red as representative of different NPQ amplitudes at the end of the actinic treatment. C) Example of NPQ kinetics obtained during 5 minutes of actinic light followed by 3 minutes of dark relaxation. Independent lines are shown in different colors and symbols.

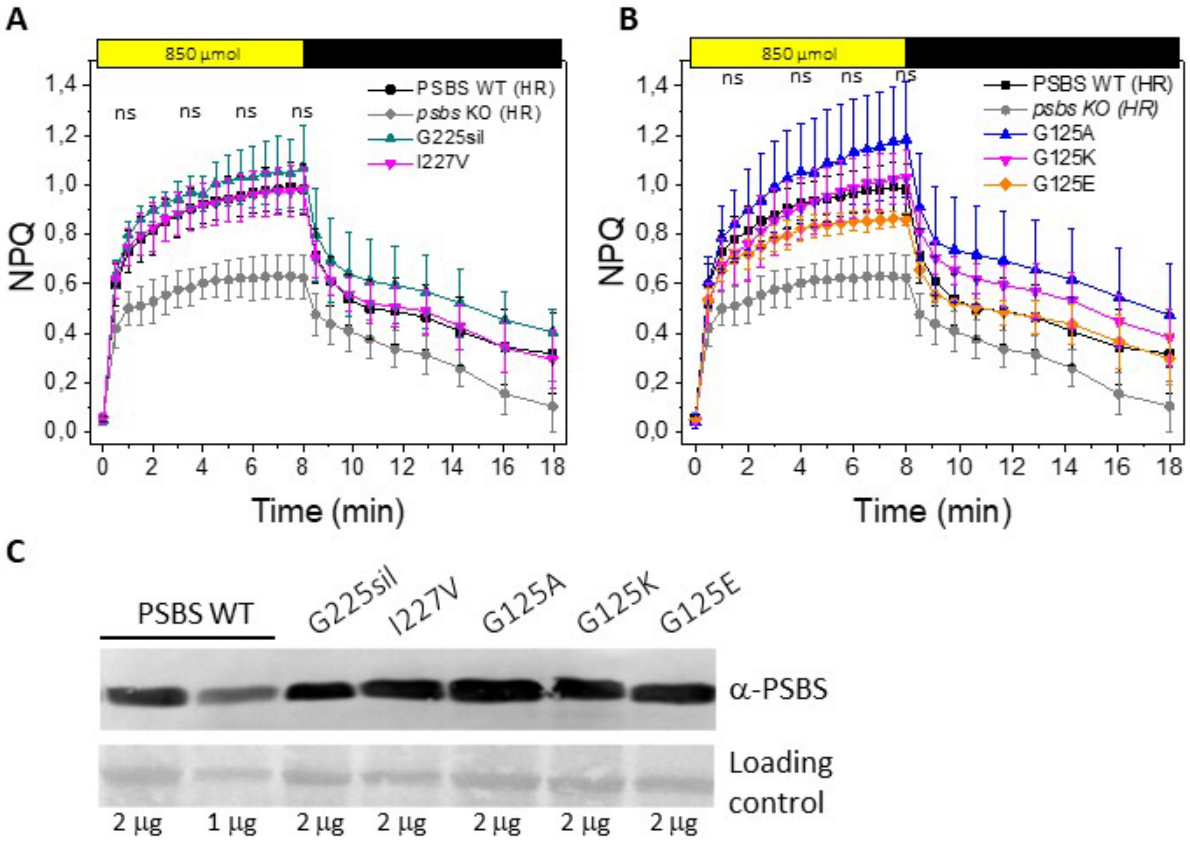

Figure 3. Mutations with no effect on NPQ activity. NPQ kinetics of different edited lines are reported along with those of *lhcsr1* KO (i.e. PSBS WT (HR), black squares) and *lhcsr1 psbs* KO (i.e. *psbs* KO (HR), grey circles). (A) NPQ kinetics of G225sil (cyan triangles) and I227V lines (magenta triangles). (B) NPQ kinetics of G125A (blue triangles), G125K (magenta triangles) and G125E lines (orange diamonds). Each line is the result of at least 3 independent biological replicates. "ns" indicates no significant differences between PSBS WT (HR) and mutant lines after One-Way ANOVA test, $p < 0,05$. (C) Immunoblot against PSBS for PSBS WT (HR) and for the lines shown in panels A and B (i.e. G225sil, I227V, G125A, G125K and G125E). Proteins equivalent to 1 or 2 µg of chlorophyll were loaded in each lane as indicated.

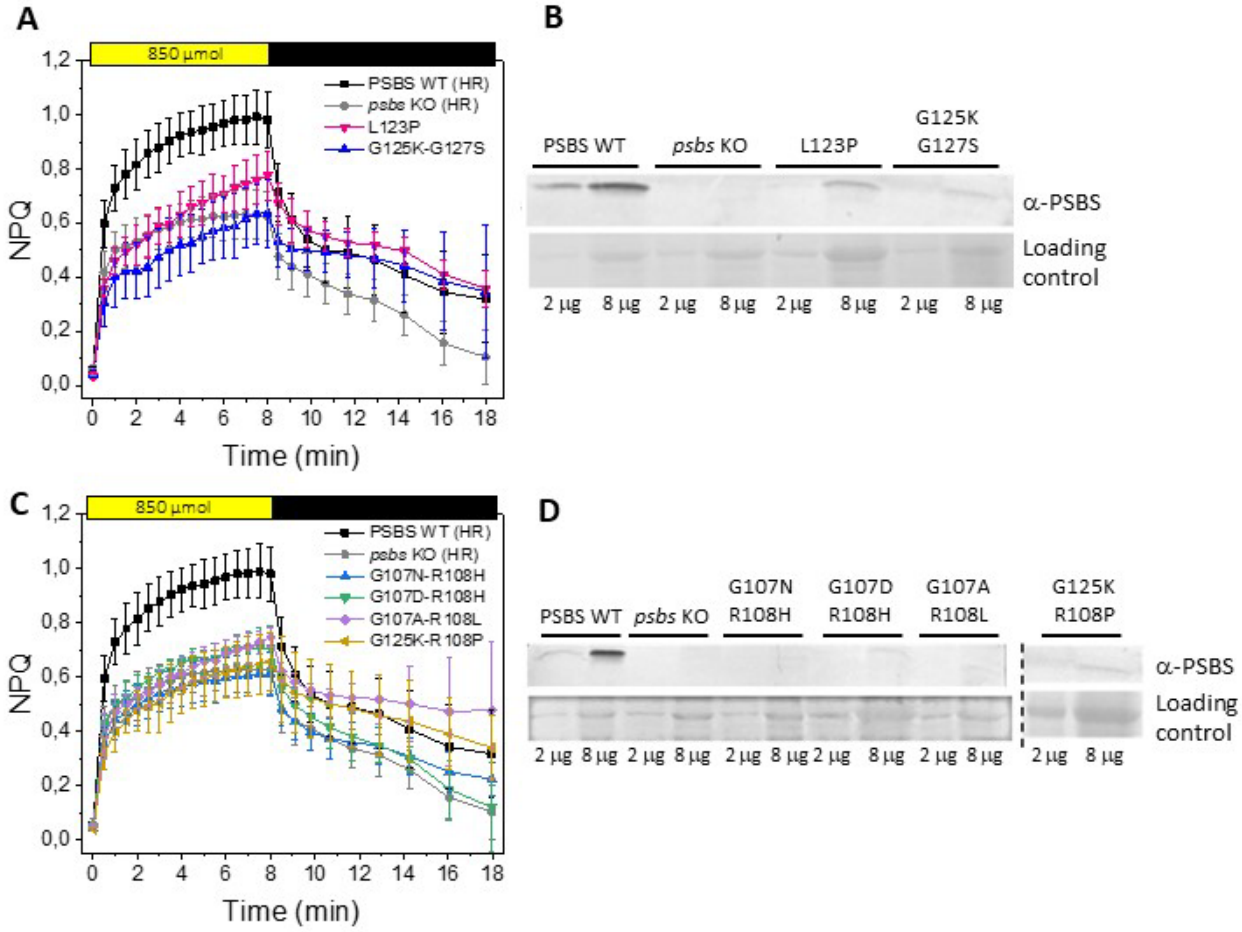

igure 4. Mutations causing PsbS protein de-stabilization. NPQ kinetics (A-C) of different edited lines reported along with reference lines *lhcsr1* KO (i.e. PSBS WT (HR), black squares) and *lhcsr1 psbs* KO (i.e. *psbs* KO (HR), grey circles). (A) NPQ kinetics of lines L123P (magenta triangles) and G125K-G127S (blue triangles) and (C) lines G107N-R108H (light blue triangles), G107D-R108H (green triangles), G107A-R108L (violet diamonds), G125K-R108P (brown triangles). For each sample, a minimum of 3 independent biological replicates were used. Immunoblot analysis (B-D) comparing PsbS accumulation in PsbS WT line, *psbs* KO line and edited lines mentioned in panels A and B. Proteins equivalent to 2 or 8 µg of chlorophyll were loaded in each lane as indicated.

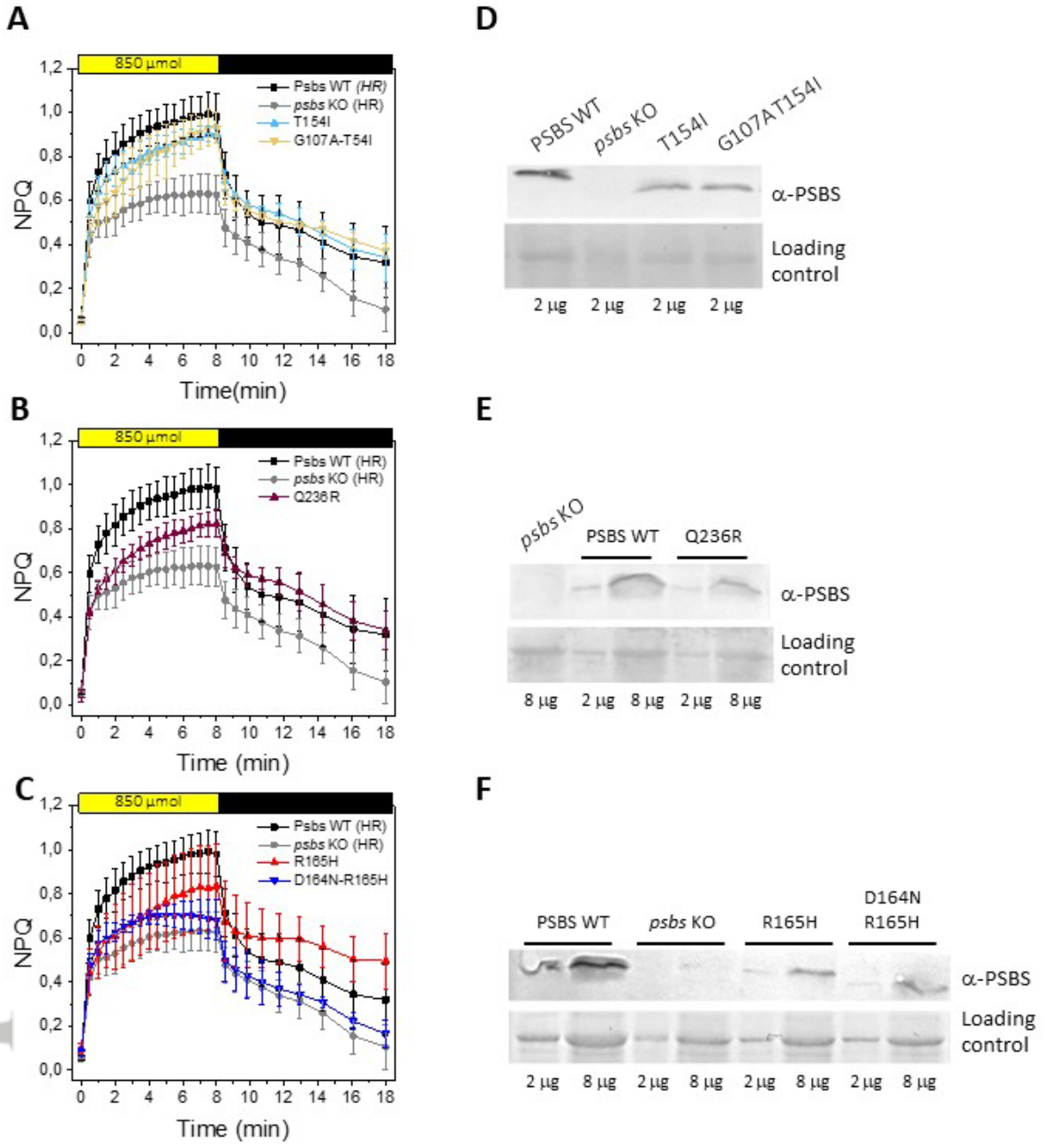

Figure 5. Lines with altered PsbS stability. NPQ kinetics of (A) T154I (blue triangles), G107A-T154I (orange triangles), (B) Q236R (brown triangles), (C) R165H (red triangles) and D164N-R165H (blue triangles) compared to *lhcsr1* KO PSBS WT (black squares) and *lhcsr1 psbs* KO (grey circles). For all plants, measurements show average of at least 3 independent biological replicates. D-F) Immunoblot analysis of the same lines reported in A-C. Proteins equivalent to 2 or 8 µg of chlorophyll were loaded in each lane as indicated.

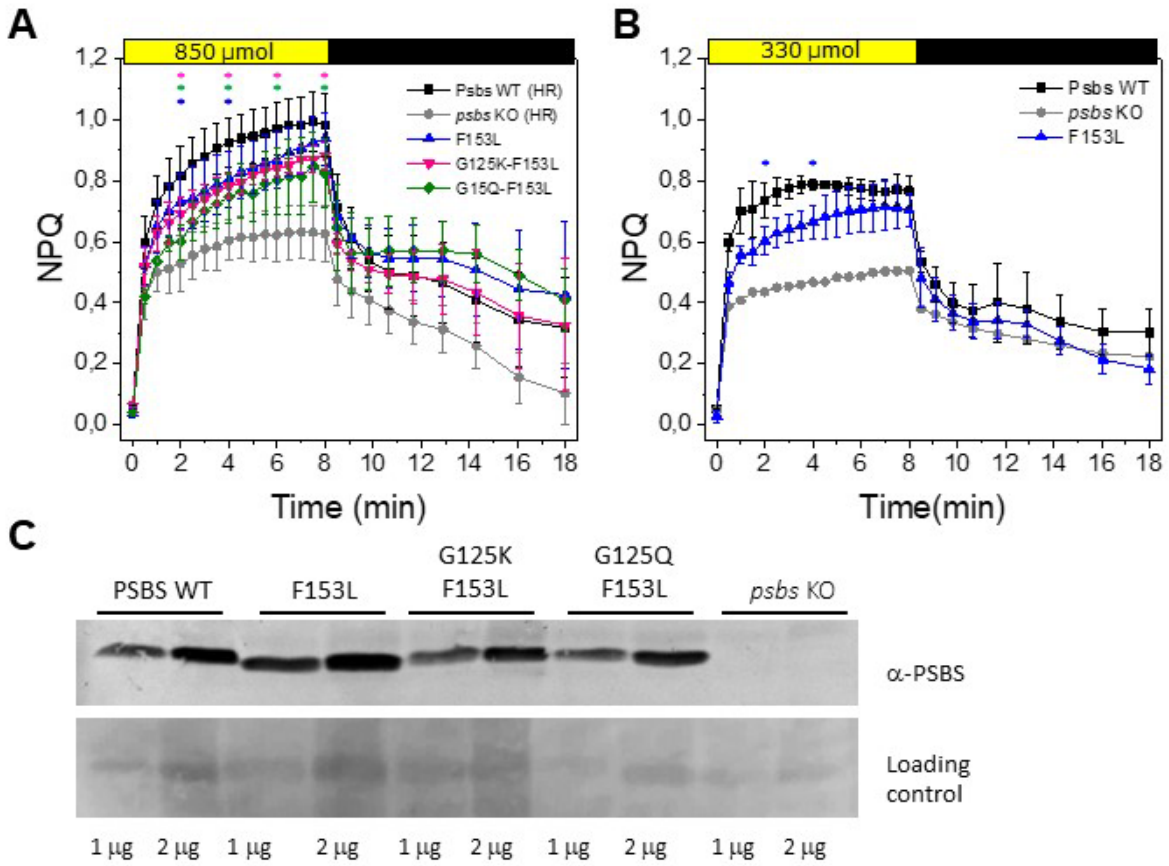

Figure 6. Lines affected in NPQ kinetic but showing unaltered protein accumulation. A-B) NPQ of F153L (blue triangles), G125K-F153L mutant (pink triangles), G125Q-F153L mutant (green diamonds) compared with *lhcsr1* KO *psbs WT* (black circles) and *lhcsr1 psbs* KO (grey circles). Two different actinic light were used, 850 µmol photons m^{-2} s^{-1} (A) and 330 µmol photons m^{-2} s^{-1} (B). Data represent average values of at least 3 biological replicates ± SD. Asterisks indicate significant differences between *psbs* WT lines and mutant lines (One-Way ANOVA p=0.05). C) Immunoblot analysis of the same lines reported in A. Proteins equivalent to 1 or 2 µg of chlorophyll were loaded in each lane as indicated.

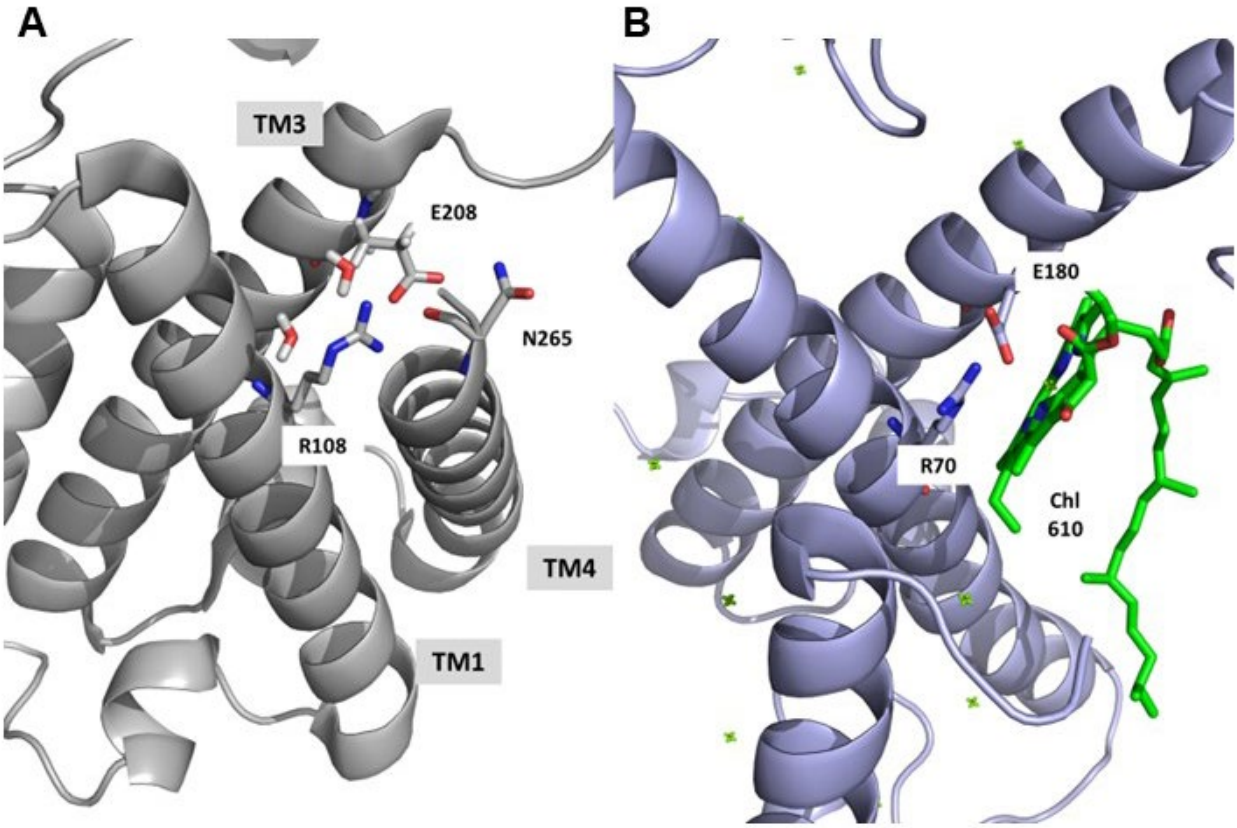

Figure 7. Hydrophilic interactions stabilizing PsbS structure. A) Overview of R108 position and polar contacts in PSBS structure. R108 is located in TM1 and its side chain interacts with two water molecules as well as E208 from TM3 and A263 and N265 from TM4. Residues are shown as sticks. Nitrogen and oxygen atoms are coloured in blue and red respectively. B) Structure of LHCII from spinach (pdb 1RWT, (Liu *et al.*, 2004)) with aligned TM helix orientation. Interactions with Psbs TM4 are substituted by Chl 610.

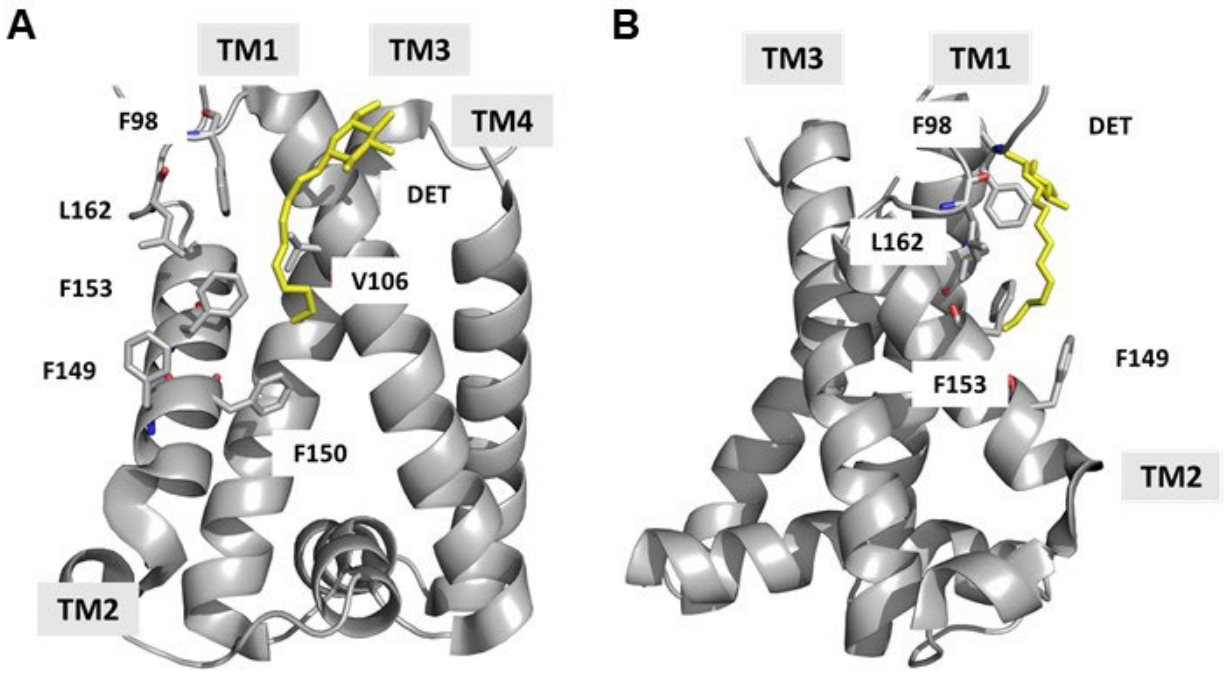

Figure 8. Overview of Psbs hydrophobic cluster. A) PsbS structure highlighting residues of hydrophobic cluster around F153. Residues are shown as sticks. Nitrogen and oxygen atoms are coloured in blue and red respectively. Detergent (DET) molecule is coloured in yellow. Different transmembrane helices (TM) are indicated. B) PsbS structure shown in panel (A) but rotated 90° counterclockwise.